# Chapter 5
# Accelerating QM/MM Calculations by Using the Mean Field Approximation

**M. Elena Martín, M. Luz Sánchez, Aurora Muñoz-Losa, Ignacio Fdez. Galván and Manuel A. Aguilar**

**Abstract** It is well known that solvents can modify the frequency and intensity of the solute spectral bands, the thermodynamics and kinetics of chemical reactions, the strength of molecular interactions or the fate of solute excited states. The theoretical study of solvent effects is quite complicated since the presence of the solvent introduces additional difficulties with respect to the study of analogous problems in gas phase. The mean field approximation (MFA) is used for many of the most employed solvent effect theories as it permits to reduce the computational cost associated to the study of processes in solution. In this chapter we revise the performance of ASEP/MD, a quantum mechanics/molecular mechanics method developed in our laboratory that makes use of this approximation. It permits to combine state of the art calculations of the solute electron distribution with a detailed, microscopic, description of the solvent. As examples of application of the method we study solvent effects on the absorption spectra of some molecules involved in photoisomerization processes of biological systems.

## 5.1 Introduction

There are many situations in which the electron distribution of molecules suffers important changes; some examples are chemical reactions, where bonds are formed or broken, or electron excitations, where large charge redistribution takes place. It is well known that a classical description (through force fields) does not reproduce adequately the charge flows that accompany these processes and the use of quantum

M.E. Martín · M.L. Sánchez · A. Muñoz-Losa · M.A. Aguilar (✉)
Área de Química Física, University of Extremadura, Avda. Elvas s/n, Edif. José Mª Vigera Lobo 3ª planta, 06006 Badajoz, Spain
e-mail: maguilar@unex.es

I. Fdez. Galván
Department of Chemistry–Ångström, The Theoretical Chemistry Programme, Uppsala University, PO Box 518, 751 20 Uppsala, Sweden



J.-L. Rivail et al. (eds.), *Quantum Modeling of Complex Molecular Systems*, Challenges and Advances in Computational Chemistry and Physics 21,
DOI 10.1007/978-3-319-21626-3_5

mechanics becomes compulsory. Luckily, in most cases, the changes in the electron distributions are limited to only a small part of the system, usually, the active center or the chromophore. In these situations the use of focused methods [1] is especially useful. In focused methods the whole system is partitioned into two parts, the part of interest or focused part and the surroundings. In general, the part of interest of the system is quantum-mechanically described while the rest of the system is classically described. Examples of focused methods are dielectric continuum methods [1–4] or quantum mechanics/molecular mechanics (QM/MM) methods [5–7].

A characteristic of liquids is that they have many thermally accessible conformations. Consequently, in the study of the properties of these systems we must resort to some of the techniques developed by statistical mechanics. The presence of a surrounding medium can have important effects on the geometry, charge distribution, reactivity and spectroscopic properties of solutes. Different solvent configurations can yield slightly different solute properties; consequently the value of any molecular property must be calculated by averaging over a large enough set of conformations or configurations.

These two factors, the great number of thermally accessible configurations and the need to describe the charge distribution changes through quantum mechanics, taken together, increase dramatically the computational cost associated to the theoretical study of chemical reactions and electron transitions of molecules in solution. Throughout the years several strategies and approximations have been proposed to tackle this problem, in this chapter we will center in the study of one of the most useful: the mean field approximation (MFA) [8–10]. It is worth noting that the MFA is always applied in conjugation with focused methods. This approximation permits to dramatically improve the computational efficiency, which explains its widely extended use for molecules and biomolecules in solution. The importance of this approximation is evidenced by the fact that it is employed by many of the most used methods for the study of solvent effects on chemical or biochemical systems. The different quantum versions of dielectric continuum models [1–4], the methods based on Langevin dipoles [11] or more elaborate methods such as RISM-SCF [12–14], Mean-Field QM/MM [15], statistically-mechanically averaged solvent density [16] or ASEP/MD [17–19] are representative examples of this.

In the following sections we will try to clarify the theoretical fundament of MFA and we will discuss some applications.

## 5.2 Methods and Details

From a conceptual point of view the MFA is very simple [20–22]: it replaces the energy obtained by averaging over a set of configurations with the energy of an average configuration. The same procedure is applied in calculating any other property. Note that in the first case we need to calculate the energy of every configuration, while with the MFA we calculate only one energy value. Obviously,

in this latter case the problem is how to determine and represent the average configuration. The important point to keep in mind when we use the MFA is that the effect of the classical subsystem, which can adopt many different configurations, on the quantum subsystem is introduced in an averaged way.

ASEP/MD, acronym for averaged solvent electrostatic potential from molecular dynamics, is a QM/MM method oriented towards the study of solvent effects that makes use of the mean field approximation. It permits to combine state of the art quantum calculations of the solute electronic wavefunction with a microscopic description of the solvent. Its main features are: (1) in optimizing the geometry and electronic structure of the solute the liquid structure is kept fixed. In the same way, when the liquid phase space is explored it is assumed that the geometry and charge distribution of the solute do not change. (2) The solute wavefunction and the liquid structure around it are optimized using an iterative procedure where a quantum calculation follows a molecular dynamics simulation. (3) The perturbation generated by the solvent on the solute enters into the molecular Hamiltonian in an averaged way. (4) The location of the critical points (minima, transition states, etc.) on the free energy surfaces is performed using a modification of the free energy gradient method.

We pass now to detail the method. Let us suppose the total system is formed by one solute molecule and N solvent molecules in a volume V. As usual in QM/MM methods the total Hamiltonian of the system is defined as:

$$\hat{H} = \hat{H}_{\mathrm{QM}} + \hat{H}_{\mathrm{class}} + \hat{H}_{\mathrm{int}} \tag{5.1}$$

corresponding to the quantum region, $\hat{H}_{\mathrm{QM}}$, the classical region, $\hat{H}_{\mathrm{class}}$, and the interaction between them, $\hat{H}_{\mathrm{int}}$. The quantum region is formed by the solute molecule and the classical one by the N solvent molecules. This distinction is important only during the quantum calculation, in the MD simulation all the molecules (solute +solvent) are classically treated.

The energy and wavefunction of the QM region are obtained by solving the effective Schrödinger equation:

$$\left(\hat{H}_{\mathrm{QM}} + \left\langle \hat{H}_{\mathrm{int}} \right\rangle\right) |\Psi\rangle = \bar{E} |\Psi\rangle \tag{5.2}$$

Here the mean field interaction Hamiltonian, $\hat{H}_{int}$, is defined as [20–22]:

$$\left\langle \hat{H}_{\mathrm{int}} \right\rangle = \int dr \cdot \hat{\rho} \cdot \langle V_S(r) \rangle \tag{5.3}$$

where $\hat{\rho}$ is the charge density operator of the quantum mechanical region (the solute) and $\langle V_S(r) \rangle$, which is named ASEP, is the average electrostatic potential generated by the solvent molecules at the position $r$. The brackets denote a statistical average over the configurational space of the classical subsystem.

In ASEP/MD, the information necessary to calculate $\langle V_S \rangle$ is obtained from a classical molecular dynamics simulation.

From a computational point of view it is convenient to split the interaction term into two components associated to the electrostatic and van der Waals contributions:

$$\hat{H}_{\text{int}} = \hat{H}_{\text{int}}^{\text{elect}} + \hat{H}_{\text{int}}^{\text{vdW}} \tag{5.4}$$

In general, it is assumed that $\hat{H}_{int}^{vdW}$ has only a small effect on the solute wavefunction and therefore it is usual to represent it through a classical potential that depends only on the nuclear coordinates but not on the electron ones. If this is the case, and for a given configuration of the classical subsystem, the $\hat{H}_{int}^{vdW}$ term can simply be added to the final value of the energy as a constant.

Equations (5.2) and (5.3) show how the classical region perturbs the quantum one and originates the solute polarization. Obviously, the classical subsystem depends in turn on the charge distribution of the quantum subsystem. As a consequence, Eq. (5.2) becomes an implicit non-linear expression that needs to be solved iteratively. At the end of this procedure, when convergence is reached, the solute charge distribution and the solvent structure around it become mutually equilibrated.

Scheme 5.1 can help to clarify the different steps of the ASEP/MD method. It begins by solving the Schrödinger equation of the isolated quantum subsystem. From this we obtain the electron distribution or any other derived quantity like the atomic point charges, etc., that are used to represent the solute in a classical molecular dynamics simulation. The ASEP calculation implies an average of the different configurations that the classical subsystem can adopt. Next, the ASEP is introduced into the molecular Hamiltonian. By solving the associated Schrödinger Eq. (5.2) we get the wavefunction of the quantum subsystem perturbed by the classical one. This perturbation modifies both the geometry and electron distribution of the quantum subsystem that consequently becomes polarized. The new charge distribution is used to recalculate the ASEP that is again introduced into Eq. (5.2). The procedure is repeated until convergence is attained, which typically occurs in a few cycles. At the end of this iterative procedure we get the energy, geometry and wavefunction of the quantum region and the structure of the classical region.

It is worth of note that most of the configurations generated in a MD simulation are not statistically independent, i.e., they do not provide additional information from a statistical point of view [23, 24]. So, in order to decrease the statistical correlation between the selected configurations it is important to include just those configurations separated by a time interval larger than the relaxation time. The length of this interval varies depending on the system under study, although intervals of at least 0.05 ps are usually needed. More important than including many configurations in the ASEP calculation is that they span a long enough simulation time (at least several hundreds of ps). In general, converged results are obtained with 500–1000 statistically independent configurations.

Another important point to clarify is what is the most adequate way of introducing ASEP into the Hamiltonian. There are several possibilities: numerically, as a set of point charges, using multipole expansions, etc. In general, we use a point charge representation, as it provides a compromise between accuracy and computational cost. The problem with this option is that the number of charges increases rapidly with the size of the system and with the number of configurations included. So, for instance, for a simulation with 500 molecules with five atoms per molecule and using 1000 configurations in the ASEP calculation we have $5 \times 500 \times 1000 = 2500000$ charges. In order to keep a tractable number of charges we include explicitly only those charges associated to molecules that belong to the first solvation shell of the solute. The effect of the remaining solvent molecules is described by using potential-fitted charges. A further charge number reduction method permits to reduce their number to only a few thousands. More details about the calculation and representation of the ASEP can be found elsewhere [17–19, 25–27].

For optimizing the geometry of the quantum system we use a variant [28] of the free energy gradient method [29–31] that permits the determination of critical points on free energy surfaces (FES). The FES is defined as the energy associated with the time average of the forces acting on the solute molecule. Let $A$ be the Helmholtz free energy of a system. The force felt by the solute molecule reads

$$\langle F(R)\rangle = -\frac{\partial A}{\partial R} = -\left\langle \frac{\partial E}{\partial R}\right\rangle = -\frac{\partial E_{QM}}{\partial R} - \left\langle \frac{\partial E_{int}}{\partial R}\right\rangle \tag{5.5}$$

**R** being the nuclear coordinates of the solute, $E$ the energy obtained as the solution of the Schrödinger Eq. (5.2), $E_{QM} = \langle \Psi | H_{QM} | \Psi \rangle$, $E_{int} = \langle \Psi | H_{int} | \Psi \rangle$ and where we have assumed that $E_{\text{class}}$ does not explicitly depend on the solute nuclear coordinates $R$ and that the geometry of the quantum part is keep fixed during the MD simulation. The brackets denote a configurational average. Note that $E$ incorporates both intramolecular, $E_{QM}$, and intermolecular, $E_{\text{int}}$, contributions.

In the same way the Hessian reads:

$$\langle G(R,R')\rangle = \left\langle \frac{\partial^2 E}{\partial R \partial R'}\right\rangle - \beta\left\langle \frac{\partial E}{\partial R}\left(\frac{\partial E}{\partial R'}\right)^T\right\rangle + \beta\left\langle \frac{\partial E}{\partial R}\right\rangle\left\langle \frac{\partial E^T}{\partial R'}\right\rangle \tag{5.6}$$

where the superscript T stands for *transpose* and $\beta = 1/k_B T$. The last two terms in Eq. (5.6) are related to the thermal fluctuations of the force.

Turning to the expression of the force, it is convenient to split the interaction term into two components associated with the electrostatic and van der Waals contributions:

$$\langle F(R)\rangle = -\frac{\partial E_{QM}}{\partial R} - \left\langle \frac{\partial E_{int}^{elect}}{\partial R}\right\rangle - \left\langle \frac{\partial E_{int}^{vdW}}{\partial R}\right\rangle \tag{5.7}$$

At this point one can introduce the MFA by replacing the average derivative of $E_{int}^{elect}$ with the derivative of the average value. The force now reads [28]:

$$\langle F(R)\rangle = -\frac{\partial E_{QM}}{\partial R} - \frac{\partial \bar{E}_{int}^{elect}}{\partial R} - \left\langle \frac{\partial E_{int}^{vdW}}{\partial R} \right\rangle \tag{5.8}$$

and, analogously, the Hessian reads:

$$\langle G(R,R')\rangle = -\frac{\partial^2 E_{QM}}{\partial R \partial R'} - \frac{\partial^2 \bar{E}_{int}^{elect}}{\partial R \partial R'} - \left\langle \frac{\partial^2 E_{int}^{vdW}}{\partial R \partial R'} \right\rangle \tag{5.9}$$

where, in agreement with the mean field approximation, the force fluctuation term has been neglected. Once the gradient and Hessian values are known, we can use any of the usual optimization methods, RFO [32] for instance, to get the optimized geometry and couple it with Scheme 5.1.

A point that deserves attention is the contribution of the electronic solvent polarization to the solvatochromic shifts. Most force fields use atomic point charges that include the effect of electron polarization in an implicit way. The main problem with the use of this implicit description of the electronic polarization is that it gives a vanishing contribution when one compares situations where the solvent structure is fixed, for instance when the Franck-Condon principle is applied in vertical transitions. In these situations it is convenient to have a model to compute explicitly

**Scheme 5.1** Scheme of the MFA iterative procedure

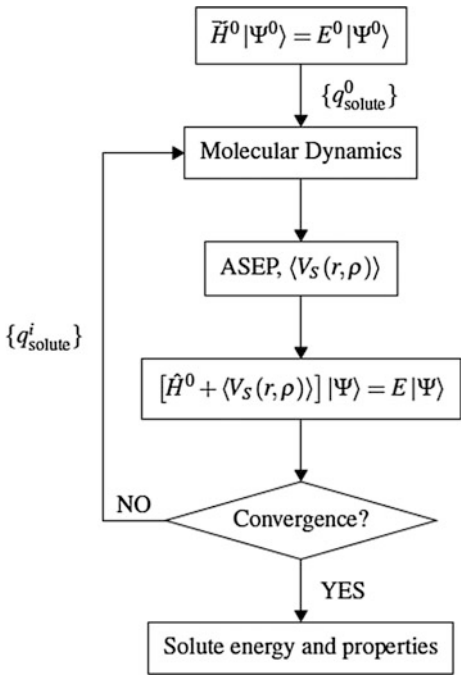

the contribution of the electronic polarization component. To this end, we assign a molecular polarizability to every solvent molecule, and simultaneously replace the effective solvent charge distribution used in the MD calculation with the gas phase values of the solvent molecule. This point is important, because otherwise the solvent polarization is accounted twice. The dipole moment induced on each solvent molecule is a function of the dipole moments induced on the rest of the molecules and of the solute charge distribution, and hence the electrostatic equation has to be solved self-consistently.

The total energy of the system (quantum solute + polarizable solvent) is obtained as:

$$U = U_{qq} + U_{pq} + U_{pp} + U_{\rho q} + U_{\rho p} + U_{dist}^{solute} + U_{dist}^{solvent} \tag{5.10}$$

Here, $q$ refers to the permanent charges of solvent molecules, $p$ to the solvent induced dipoles, and $\rho$ is the solute charge density. The last two terms in this equation are the distortion energies of the solute and solvent molecules respectively, i.e., the energy spent in polarizing them. In the case of the solute it reads:

$$U_{dist}^{solute} = \left\langle \Psi \middle| H_{QM} \middle| \Psi \right\rangle - \left\langle \Psi^0 \middle| H_{QM} \middle| \Psi^0 \right\rangle \tag{5.11}$$

where $\Psi$ and $\Psi^0$ are the in solution and in vacuo solute wave-functions, respectively. Explicit expressions for the different contributions can be found elsewhere [26].

The final expression for the total energy of the system is:

$$U = U_{qq} + \frac{1}{2} U_{pq} + + U_{\rho q} + \frac{1}{2} U_{\rho p} + U_{dist}^{solute} \tag{5.12}$$

The firsts two terms of this expression are strictly classical, while the last three involve the solute charge distribution and are calculated quantum-mechanically.

Finally, we address the application of the ASEP/MD methodology to the study of electronic transitions. Here, we can consider two situations depending on the description, implicit or explicit, of the solvent electronic polarization. If one uses an implicit description of this component then it is only necessary to perform the calculation of the different excited states in presence of the solvent charge distribution obtained during the ASEP/MD procedure. If, on the contrary, we explicitly include the contribution of this component then it is necessary to perform an additional self-consistent process. Using the solvent structure and solute geometry obtained in the first self-consistent process, we couple the quantum mechanical solute and the electron polarization of the solvent. The process finishes when the solute charge distribution and the solvent induced dipole moments become mutually equilibrated.

Once the solvation energy, Eq. (5.12), has been calculated for the ground and excited states, the solvent shift, $\delta$, can be obtained as the difference

$$\delta = U_{ex} - U_g = \frac{1}{2}\delta_{pq} + \delta_{\rho q} + \frac{1}{2}\delta_{\rho p} + \delta_{dist}^{solute} \tag{5.13}$$

The term $\delta_{qq}$ cancels out because, in vertical transitions where the Franck-Condon approximation is applicable, the $U_{qq}$ term takes the same value in both the ground and the excited state.

A problem with this procedure is that the solvent perturbs each electronic state of the solute molecule in a different way, i.e., each state is an eigenfunction of a different Hamiltonian; consequently, the different states are not mutually orthogonal. This fact complicates the calculation of oscillator strength and other transition properties of the system.

## 5.3 Examples

In this section we present results of the application of the ASEP/MD method to the study of solvent effects on electron transitions in p-coumaric acid derivatives. This system was chosen because it is an example of electron excitations that promote internal rotation around formal double bonds. Internal rotations are characterized by large flows of charge and, consequently, important solvent effects. Furthermore, they are involved in very interesting phenomena, as are dual fluorescence in push-pull chromophores [33–35] or *cis-trans* photoisomerization reactions [36–38]. An adequate description of the excited states involved in these processes demand state of the art quantum calculations including both static and dynamic electron correlation contributions. Furthermore, in many cases the solute is stabilized by hydrogen bonds, consequently, it is compulsory to use a microscopic description of the solvent in order to account for specific interactions. In these conditions ASEP/MD becomes a good alternative to other methods and it can help to shed light on these processes [39–42].

### *5.3.1 p-Coumaric Acid in Different Protonation States*

p-coumaric acid (pCA) has been used as a model of the photoactive yellow protein (PYP) chromophore. This protein is related with the negative phototaxis of *Halorhodospira halophila* under blue light irradiation [38]. After irradiation (446 nm), the protein enters a photocycle where the primary event is the isomerization of the chromophore's double bond on a subpicosecond time scale, very similar to retinal photoisomerization in the visual process [43–46]. A first evidence of the medium effect on the p-coumaric acid chromophore is found in the absorption spectrum. In gas phase, the p-coumaric monoanion ($pCA^-$) absorbs at 430 nm [47, 48] whereas in water solution the absorption maximum is located at

around 310 nm and it varies with the pH [48, 49]. It is important to note that pCA has two hydrogen atoms susceptible of deprotonation being the carboxylic hydrogen more acid than the phenolic one. Thus, in passing from acidic to neutral condition, the chromophore will first lose the carboxylic hydrogen yielding the carboxylate anion rather than the phenolate. Nevertheless, in gas phase, the phenolate anion is found to be more stable than the carboxylate due to the delocalization the negative charge along the structure. At basic pH the dianionic form is obtained.

In this section we compare the absorption spectra of p-coumaric acid as a function of its protonation state. During the ASEP/MD runs, quantum calculations were performed with the Gaussian 09 package [50]. The final SA-CASSCF and CASPT2 calculations were done with Molcas 7.4 [51]. All MD simulations were performed using Moldy [52] or Gromacs [53] and assuming rigid molecules. Lennard-Jones parameters and solvent atomic charges were taken from the OPLS-AA (optimized potentials for liquid simulations, all atoms) force field [54, 55]. Solute atomic charges were obtained from the quantum calculations with the CHELPG (charges from electrostatic potential in a grid) method [56, 57].

We started our study with the neutral form of the *trans*-pcoumaric acid (pCA). Four conformes were studied. Two of them correspond to the *cis* or *trans* disposition of the central vinyl double bond and the carboxylic double bond of the acid terminal group, s-*cis* and s-*trans*. For each of these species, the hydrogen of the phenolic group can be disposed in syn or anti position relative to the central double bond. These four species are displayed in Scheme 5.2 and are identified as I (s-*cis*-anti), II (s-*cis*-syn), III (s-*trans*-anti) and IV (s-*trans*-syn). In gas phase, anti rotamers are preferred to the syn ones, in solution the opposite is verified and the syn conformations are slightly more stable than anti.

Regarding the absorption spectrum, the most probable transition in gas phase is a ($\pi \rightarrow \pi^*$) absorption to the $S_2$ state with an oscillator strength of around 0.5. This is

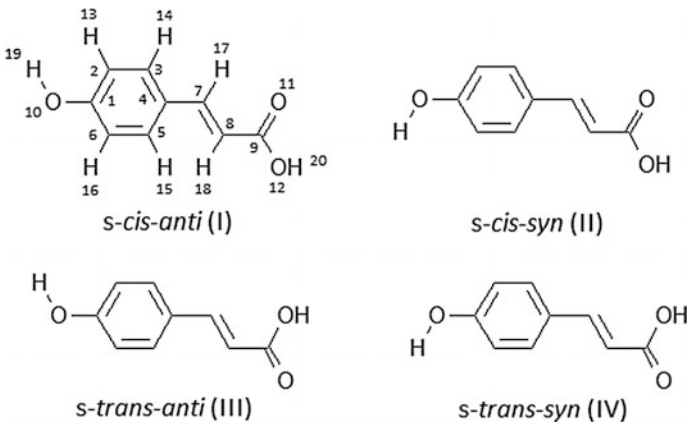


**Scheme 5.2** Conformers for the neutral form of the *trans*-p-coumaric acid

a HOMO→LUMO transition involving a gap of 4.5 and 4.6 eV for the s-*cis* and s-*trans* isomers, respectively. The transition to the $S_1$ state corresponds to a HOMO→LUMO+1 transition with an energy gap of around 4.23 eV for all the forms.

In water, the most probable transition is still that corresponding to the $S_2$ state, with an oscillator strength of 0.4. This transition results in around 4.30 eV, which overestimates the experimental value in about 0.3 eV. However, if the solvent electronic polarization is explicitly considered we get a value of 4.00 eV, in perfect agreement with the experiment. It is also observed that the $S_0 \rightarrow S_1$ transition is hardly affected by the solvent interaction, being the vertical transition energies in gas phase and in solution practically coincident. The different behavior of $S_2$ and $S_1$ comes from the distinct charge distribution of these states. Whereas the transition to $S_2$ implies an electron density displacement from the phenolic ring to the alkyl fragment and a considerable increase in the dipole moment, $S_1$ has a charge distribution similar to $S_0$ and consequently they interact with the solvent in a similar way. Due to the larger stabilization of $S_2$ with respect to $S_1$ in water solution the relative stability order of the two states is reversed.

The situation is somewhat more complicated for the monoanionic form of p-coumaric acid ($pCA^-$) as it can appear (see Scheme 5.3) in two forms: phenolate and carboxylate, with very different charge distributions. So, whereas in the carboxylate the negative charge is localized on the carboxylate end, in the phenolate anion, the negative charge is spread along the whole molecule. In fact, in phenolate, there is an equilibrium between a quinolic structure with the negative charge localized at the COOH fragment, and a nonquinolic structure with the negative charge at the phenolate oxygen. In gas phase, the ground state of the phenolate form is clearly more stable than the carboxylate species due to its larger charge delocalization. Interaction with solvent molecules modifies the relative stability of the different isomers, and in water solution, the carboxylate becomes now the most stable form.

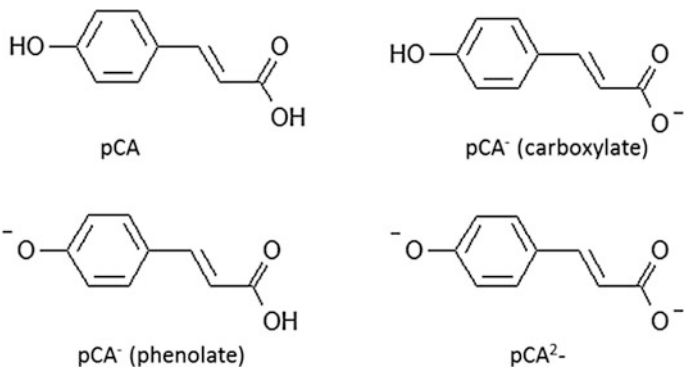


**Scheme 5.3** Neutral, monoanionic and dianionic forms of the *p*-coumaric acid

An additional complication comes from the fact that for both carboxylate and phenolate monoanions, the gas-phase ($\pi \rightarrow \pi^*$) low-lying excited states are found in the detachment continuum [58–60], that is, their electron detachment energies are below the first vertical excitation energy, and therefore, these excited states are metastable. In any case, there is a very good agreement between the calculated CASPT2/CASSCF(12,24) gas phase excitation energy for phenolate (2.89 eV) and the experimental data (2.88 eV).

The most probable transition in gas phase is that leading to the $S_1$ state, with an oscillator strength of 1.0. In water solution, the bright state remains $S_1$, with the same nature as in gas phase. The absorption band appears displaced toward larger energies (3.17 or 3.09 eV depending whether the solvent is explicitly polarized or not); consequently, there is a blue solvent shift of around 0.25 eV.

The theoretical electronic absorption spectrum of the carboxylate anion is quite complex due to the large number of excited states lower in energy than the bright one. In fact, the transition with the larger oscillator strength (0.50) is $S_0 \rightarrow S_4$. This corresponds to a ($\pi \rightarrow \pi^*$) transition involving the HOMO and LUMO orbitals. We find a difference of 2.1 eV between the gas-phase transition energies of carboxylate (5.06) and phenolate (2.89). In water solution, the bright state is the $S_2$ excited state. It is a H→L transition, and it has an oscillator strength slightly larger than that found in gas phase. This state is more effectively solvated and more stabilized than the ground state, the transition energy is 4.76 eV and a red solvent shift of 0.3 eV is found. Explicit inclusion of the electronic solvent polarization slightly increases the transition energy until 4.81 eV.

The double anionic form of the trans-p-coumaric acid ($pCA^{2-}$) is unstable in gas phase and would suffer spontaneous autoionization. However, the interaction with the solvent increases the ionization potential permitting the existence of $pCA^{2-}$ in water solution. In gas phase, the bright state is the $S_2$ state that corresponds to a H→L transition, whereas the $S_1$ state implies the transition H→L+1. In solution, the bright excited state is stabilized and becomes the first excited state as the charge displacement involved in this transition (−0.35 e in solution) is favored by the solvent. The calculated transition energy in solution (3.75 and 3.73 eV for non-polarizable and polarizable solvent, respectively) is in very good agreement with the experimental data recently published by Boggio-Pasqua and Groenhof [61] where the *trans*-p-coumaric acid in aqueous solution at pH > 10 showed an absorption maximum at around 3.71 eV.

The variation of the transitions energies with the protonation state is displayed in Fig. 5.1. For all the studied species, the bright state is a $\pi \rightarrow \pi^*$ transition involving a charge displacement along the system. For the neutral form, the transition involves an increase of the dipole moment of the excited state, a fact that leads to a larger stabilization of the excited state in water solution and consequently a bathochromic shift of the absorption maximum in solution. Phenolate and carboxylate monoanions show different behavior with respect to solvation. On the one hand, the phenolate monoanion in gas phase shows a displacement of the charge from the phenolic oxygen to the rest of the system during the transition, and this is enhanced in water solution. As the displacement involves a delocalization of the negative

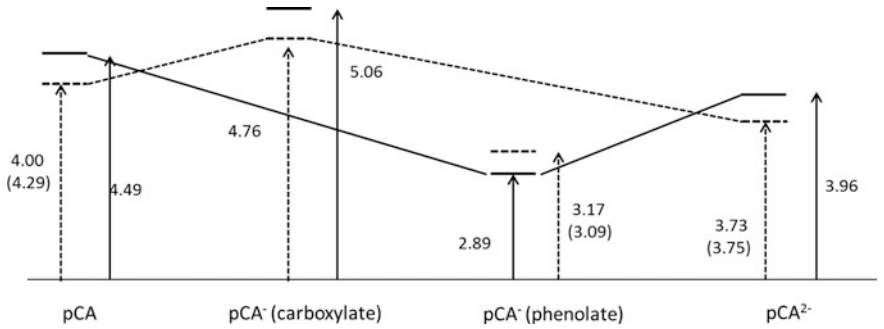


**Fig. 5.1** Variation of the transition energies (in eV) for the *trans*-p-coumaric acid with the protonation state in gas phase (*full lines*) and in water solution (*dashed lines*). For the in-solution transition energies, the effect of the electronic solvent polarization has been included (values in parentheses correspond to those obtained without this contribution)

charge, the excited state is worse stabilized than the ground state, and a final solvent blue shift is achieved. On the other hand, in the carboxylate monoanion the negative charge moves from the $COO^-$ toward the phenolic ring during the excitation. As the solvent hinders this displacement the excited state charge becomes more localized in solution, and consequently more stabilized than the ground state and a solvent red shift is found. Finally, for the dianionic species the electronic transition to the bright state involves a charge displacement from the phenolic part toward the rest of the system and most of the negative charge is concentrated in the carboxyl end. This displacement is enhanced in water solution; as a consecuence, the charge is more localized and more effectively solvated in the excited state than the ground state, and a final solvent red shift is found. In sum, except for the phenolate anion where a blue shift is found in the rest of cases a blue shift is registered.

As for the effect of the electronic solvent polarization in the transition energies and solvent shift values two cases can be distinguished. In neutral species, the polarization contribution depends on the state nature. That is, it is relevant in those cases in which there exists a significant charge displacement between the ground and the excited state. On the contrary, in ionic forms (mono- and dianionic species), the larger contribution to the solute-solvent interaction energy comes from the charge−potential term and, in general, solvent polarization has only a minor influence.

Finally, we would like to draw the attention to some attempts to mimic the solvent environment effect by including a limited number of solvent molecules in the quantum calculation. Putschögl et al. [62], for instance, studied the $pCA^{2-}$ dianion surrounded by eight water molecules. They found that the solvent stabilization was not enough to cause the inversion between $S_1$ and $S_2$ states in solution, something that occurs when bulk solvation is accounted. In our case, the $S_1$ bright state is more stabilized than the ground state and consequently a red solvent shift of around 0.22 and 0.23 eV (nonpolarizable and polarizable solvent, respectively) is

obtained in water solution. This fact evidences the importance that the bulk solvent contribution has in this system.

### 5.3.2 p-Coumaric Acid Derivatives

In this section we focus on the analysis of the solvent effect and coumaryl tail on the absorption spectrum of some p-coumaric derivatives: acid ($pCA^-$), thioacid ($pCTA^-$), methyl ester ($pCMe^-$) and methyl thioester ($pCTMe^-$), see Scheme 5.4. The comparison of the behavior of these systems permits to analyze the modifications introduced by the substitution of a sulfur by an oxygen atom and the influence of the methyl group. As we will show the presence of the sulfur modulates the solvent effect, as a consequence the first two excited states become practically degenerated for pCA- and pCMe- but moderately well separated for pCTA- and pCTMe-.

In gas phase and for the four derivatives (see Table 5.1) the bright state is the first excited state with a $\pi - \pi^*$ character and oscillator strength close to one. The second excited state is a $n - \pi^*$ state that involves the phenolic oxygen lone pair and the third one corresponded to a $\pi - \pi_2^*$ transition. A good agreement was found between the calculated transition energies and the available experimental data. So, the absorption maximum for the methyl ester derivative is experimentally found at 2.88 eV [63] whereas our CASPT2//CASSCF(14,12) value is 2.94. Explicit solvent electronic polarization was not considered, as its contribution is negligible for monoanionic derivatives. For the thiophenyl ester ($pCT^-$) the transition is experimentally found at 2.70 eV [64]. This value is a good reference for $pCTMe^-$ where we found a transition energy of 2.73 eV as the electron conjugation does not extend

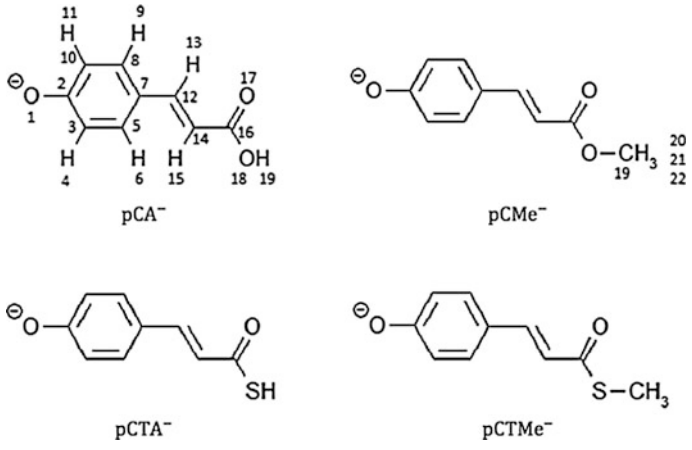


**Scheme 5.4** Acid ($pCA^-$), thioacid ($pCMe^-$), methyl ester ($pCTA^-$) and methyl thioester ($pCTMe^-$) derivatives of the anionic p-coumaric acid

**Table 5.1** Solute-solvent Interaction energies (kcal/mol) in the ground state and excited state

| | GS | | | | | $\pi \rightarrow \pi_1^*$ | | | | |
|---|---|---|---|---|---|---|---|---|---|---|
| | O- | -Ph | C = C | COXY | Total | O- | -Ph | C = C | COXY | Total |
| pCA- | −158.4 | 16.8 | −6.4 | −24.6 | −172.6 | −139.8 | 34.5 | −17.6 | −27.6 | −150.5 |
| pCMe- | −149.1 | 14.2 | −10.7 | −10.3 | −155.9 | −131.8 | 31.5 | −21.8 | −13.3 | −135.4 |
| pCTA- | −147.5 | 9.4 | 2.2 | −15.4 | −151.3 | −129.0 | 24.6 | −7.3 | −18.2 | −129.9 |
| pCTMe- | −148.5 | 12.5 | −4.2 | −5.6 | −145.8 | −131.4 | 25.8 | −13.5 | −8.1 | −127.2 |

beyond the sulfur atom. Our results also agree with the values published by Zuev et al. [65], 2.98 eV, using a similar level of calculation (SS-CASPT2/ANO-RCC-VTZP) and by Gromov et al. [66], 2.89 eV, using CC2/SV(P). The TDDFT method overestimates excitation energies. So, Muguruza González et al. [67] reported values of 3.40 eV for the vertical energies of $pCTMe^-$ and Sergi et al. [68] a value of 3.24 eV for $pCA^-$. According to these values it seems evident the poor performance of TDDFT in describing charge-transfer excited states.

The replacement of oxygen by sulfur results in a red shift of the first absorption band of around 0.21 eV. However, the substitution of the terminal hydrogen for the methyl group does not modify the band position. In the four derivatives there is a flux of charge from the phenolic part toward the rest of the molecule. This flux is larger in $pCA^-$ and $pCMe^-$, ≈0.22 e, than in $pCTA^-$ and $pCTMe^-$, ≈0.13 e. Consequently, the delocalization of the charge is larger in the excited state of the oxo derivatives that becomes more stable than the thio derivatives.

The solvent has important effects on the geometry of the four models analyzed: bond lengths are notably different in gas phase and in solution. So, for instance, the phenolic oxygen bond length increases from 1.23 to 1.28 Å when one passes from gas phase to water solution. In addition, there is a certain loss of the quinolic character displayed in gas phase, single bonds becoming now longer and double bonds shorter. However, and contrary to what could be expected, the carboxylic double bond length is not modified by the solvent, probably because of the steric hindrance and the low charge on this group (C16O17).

In the ground state of the four studied molecules the solvent originates a flux of negative charge toward the phenolic moiety. However, during the excitation the flux goes from the phenolic part (0.32 e) to the central double bond (0.24 e) and the terminal moieties (0.08 e). As a consequence the negative charge in the excited states is smoothed out along the molecule. The solvent penalizes the charge delocalization in the two excited states and originates a blue shift. The destabilization is larger for the $n \rightarrow \pi^*$ state, which becomes the third excited state. The $\pi \rightarrow \pi^*$ state is also destabilizated with respect to the $\pi \rightarrow \pi_2^*$ state and more in $pCA^-$ and $pCMe^-$ than in $pCTA^-$ and $pCTMe^-$; consequently, while in the first case the S1 and S2 states become practically degenerated, in $pCTA^-$ and $pCTMe^-$ there is a gap of around 0.35 eV.

A quantity that can be useful in the analysis of solvent effects is the group contribution to the solute-solvent interaction energy (Table 5.1). The molecules are divided in portions and their relative contribution to the interaction energy and solvent shift are analyzed. In the present case we divided the molecules in four parts: the phenolic oxygen, the phenyl group, the central double bond and the terminal part (acid, thio-acid, ester or thio-ester depending on the case). The larger contribution to the total interaction energy comes from the phenolic oxygen that is the group that carries most of the negative charge. However, the contributions of the remaining groups are far from negligible. Electronic transition results in a decrease of the solute-solvent interaction energy. This is mainly due to the decrease of circa 35–40 kcal/mol in the contribution of the phenolic part of the molecule (Ph-O) as consequence of the charge flux from the phenolic part toward the rest of the molecule. The phenyl and carbonyl groups present a reduced number of water molecules placed in their neighborhood compared to those existing around the phenolic oxygen, and consequently the solvent does not stabilize the transferred charge as effectively.

It is interesting to compare ASEP/MD results with those obtained by other authors using different methodologies. So, Gromov et al. [66] calculated a CC2/aug-*cc*-pVDZ value of 2.96 eV for the transition energy of $pCTMe^-$ with two water molecules placed close to the phenolic oxygen (the part of the molecule with the largest interaction energy). This value is in reasonable agreement with the experimental value of 3.22 eV published by Naseem et al. [69]. Nevertheless, those authors report a theoretical solvent shift of 0.05 eV as they found the absorption band in gas phase at 2.91 eV. This value is clearly underestimated when compared with the experiment. Assuming the gas phase experimental value for $pCT^-$ (2.70 eV) as suitable value as well for $pCTMe^-$, the experimental solvent shift can be estimated in 0.52 eV. Furthermore, the solvent effect on the bond length variations reported by these authors represents only one-third of that obtained with ASEP/MD. The situation is even worse when the solvent is described using continuum methods as they fail in reproducing the correct trend, which is a blue solvent shift. For instance, Wang [70]. performed a CPCM/TD-B3LYP study of $pCTMe^-$ in different media. In water, the absorption energy was estimated in 3.03 eV being this value lower than the one computed in gas phase (3.17 eV). Consequently a final red shift was obtained. In this case, the failure in predicting the solvent shift is due to the neglecting by continuum models of specific solvent interaction such as hydrogen bonding. Therefore, we must conclude that the representation of the solvent through a few solvent molecules or making use of continuum methods does not accurately account for the solvation effects on the studied systems. In the first case because solvation is a global property hardly represented just through a few solvent molecules and in the second because specific interactions between solute and solvent are missing.

## 5.4 Conclusions

Microscopic solvent effect theories imply an extensive sampling of the configurational space of the solute–solvent system. Furthermore, most of processes of chemical interest involve large charge redistribution and its study requires the use of high-level quantum-mechanical methods with the consequent increase in the computational cost. The mean field approximation provides a way of reducing the number of quantum calculations and, consequently, it permits to reduce the computational cost associated with the inclusion of solvent effects. In this chapter the theoretical basis of this approximation have been analyzed. We have paid special attention to the ASEP/MD method that implements this approximation in QM/MM methods.

The main characteristics of ASEP/MD are: (1) A reduced number of quantum calculations, that permits to increase the description level of the solute electronic structure which, in fact, can be described at the same level as in gas phase studies. (2) Since the solvent is described through MM force fields, there exists a great flexibility to include both bulk and specific interactions into the calculations. (3) At the end of the procedure the solute wavefunction and the solvent structure become mutually equilibrated, i.e., the solute is polarized by the solvent and the solvent structure is in equilibrium with the polarized solute charge distribution. (4) Finally, the method permits to perform in an efficient way optimizations on free energy surfaces.

In this chapter we have presented some applications of the ASEP/MD method to the study of electron transitions that promote internal rotation around formal double bonds. More specifically we have addressed the solvent effects on the electronic spectrum of the p-coumaric acid. Important differences in facing the solvent were verified depending on the protonation state of the acid and the nature of the terminal group.

## References

1. Tomasi J, Mennucci B, Cammi R (2005) Quantum mechanical continuum solvation methods. Chem Rev 105:2999–3093
2. Cramer CJ, Truhlar DG (1999) Chem Rev 99:2161
3. Rivail JL, Rinaldi D (1976) Chem Phys 18:233–242
4. Ruiz-López MF (2008) In: solvation effects on molecules and biomolecules: computational methods and applications. In: Canuto S (ed) Springer series: Challenges and advances in computational chemistry and physics, Springer
5. Warshel A, Levitt M (1976) J Mol Biol 103:227–249
6. Singh UC, Kollman PA (1986) J Comput Chem 7:718–730
7. Field M J, Bash PA, Karplus M (1990) J Comput Chem 11(6):700–733
8. Sánchez ML, Martín ME, Galván IF, Olivares del Valle FJ, Aguilar MA (2002) J Phys Chem B 106:4813

9. Martín ME, Sánchez ML, Corchado JC, Muñoz-Losa A, Galván IF, Olivares del Valle FJ, Aguilar MA (2011) Theor Chem Acc 128:783–793
10. Yamamoto T (2008) J Chem Phys 129:244104
11. Warshel A (1991) Computer modelling of chemical reactions in enzymes and solutions. Wiley Interscience Publication, New York
12. Ten-no S, Hirata F, Kato S (1993) Chem Phys Lett 214:391
13. Sato H, Hirata F, Kato S (1996) J Chem Phys 105:1546
14. Hirata F (ed) (2003) Molecular theory of solvation (understanding chemical reactivity). Springer, Berlin
15. Nakano H, Yamamoto T (2013) J Chem Theory Comput 9:188–203
16. Kaminski JW, Gusarov S, Kovalenko A, Wesolowski TA (2010) J Phys Chem A 114:6082
17. Sánchez ML, Aguilar MA (1997) Olivares del Valle FJ. J Comput Chem 18:313
18. Sánchez ML, Martín ME, Aguilar MA (2000) Olivares del Valle FJ J Comput Chem 21:705
19. Galván IF, Sánchez ML, Martín ME, Olivares del Valle FJ (2003) Aguilar MA Comput Phys Commun 155:244
20. Tapia O (1991) In: Maksic ZB (ed) Theoretical treatment of large molecules and their interactions, vol 4. Springer, Berlin, p 435
21. Angyán JG (1992) J Math Chem 10:93
22. Sánchez ML, Aguilar MA, Olivares del Valle FJ (1997) J Comput Chem 18:313
23. Canuto S, Coutinho K (1997) Avd Quantum Chem 28:89
24. Coutinho K, Oliveira MJ et al (1998) Int J Quantum Chem 66:249
25. Martín ME, Sánchez ML, Olivares del Valle FJ, Aguilar MA (2002) J Chem Phys 116:1613
26. Martín ME, Muñoz Losa A, Galván IF, Aguilar MA (2003) J Chem Phys 118:255
27. Galván IF, Martín ME, Aguilar MA (2004) J Comput Chem 25:1227
28. Galván IF, Sánchez ML, Martín ME, Olivares del Valle FJ, Aguilar MA (2003) J Chem Phys 118:255
29. Okuyama-Yoshida N, Nagaoka M, Yamabe T (1998) Int J Quantum Chem 70:95
30. Okuyama-Yoshida N, Kataoka K, Nagaoka M, Yamabe T (2000) J Chem Phys 113:3519
31. Hirao H, Nagae Y, Nagaoka M (2001) Chem Phys Lett 348:350
32. Banerjee A, Adams N, Simons J, Shepard R (1985) J Phys Chem 89:52
33. Lippert E, Lüder W, Moll F, Nägele W, Boos H, Prigge H, Seibold-Blankenstein I (1961) Angew Chem 73:695–706
34. Rotkiewicz K, Grellmann KH, Grabowski ZR (1973) Chem Phys Lett 19:315–318
35. Grabowski ZR, Rotkiewicz K, Rettig W (2003) Chem Rev 103:3899–4032
36. Kukura P, McCamant DW, Yoon S, Wandschneider DB, Mathies RA (2005) Science 310:1006
37. Muñoz Losa A, Martin ME, Galván IF, Sánchez ML, Aguilar MA (2011) J Chem Theory Comput 7:4050–4059
38. Meyer TE (1985) Biochim Biophys Acta 806:175
39. Muñoz-Losa A, Galván IF, Aguilar MA, Martín ME (2007) J Phys Chem B 111:9864–9870
40. Muñoz-Losa A, Martín ME, Galván I, Sánchez ML, Aguilar MA (2011) J Chem Theory Comput 7:4050–4059
41. Muñoz-Losa A, Galván IF, Aguilar MA, Martín ME (2013) J Chem Theory Comput 9:1548–1556
42. García-Prieto FF, Galván IF, Muñoz-Losa A, Aguilar MA, Martín ME (2013) J Chem Theory Comput 9:4481–4494
43. Kort R, Vonk H, Xu X, Hoff WD, Crielaard W, Hellingwerf K (1996) J FEBS Lett 382:73
44. Xie A, Hoff WD, Kroon AR, Hellingwerf K (1996) J Biochem 35:14671
45. Unno M, Kumauchi M, Sasaki J, Tokunaga F, Yamaguchi S (2000) J Am Chem Soc 122:4233
46. Genik UK, Soltis SM, Kuhn P, Canestrelli IL, Getzoff ED (1998) Nature 392:206
47. Rocha-Rinza T, Christiansen O, Rajput J, Gopalan A, Rahbek DB, Andersen LH, Bochenkova AV, Granovsky AA, Bravaya KB, Nemukhim AV, Chistiansen KL, Nielsen MB (2009) J Phys Chem A 113:9442

48. Nielsen IB, Boyé-Péronne S, El Ghazaly MOA, Kristensen MB, Nielsen SB, Andersen LH (2005) Biophys J 89:2597
49. Putschögl M, Zirak P, Penzkofer A (2008) Chem Phys 343:107
50. Frisch MJ, Trucks GW, Schlegel HB, Scuseria GE, Robb MA, Cheeseman JR, Zakrzewski VG, Montgomery JA Jr, Stratmann RE, Burant JC, Dapprich S, Millam JM, Daniels AD, Kudin KN, Strain MC, Farkas O, Tomasi J, Barone V, Cossi M, Cammi R, Mennucci B, Pomelli C, Adamo C, Clifford S, Ochterski J, Petersson GA, Ayala PY, Cui Q, Morokuma K, Malick DK, Rabuck AD, Raghavachari K, Foresman JB, Cioslowski J, Ortiz JV, Stefanov BB, Liu G, Liashenko A, Piskorz P, Komaromi I, Gomperts R, Martin RL, Fox DJ, Keith T, Al-Laham MA, Peng CY, Nanayakkara A, Gonzalez C, Challacombe M, Gill PMW, Johnson BG, Chen W, Wong MW, Andres JL, Head-Gordon M, Replogle ES, Pople JA (1998) Gaussian 98, revision A11.3. Gaussian, Inc., Pittsburgh
51. Andersson K, Barysz M, Bernhardsson A, Blomberg MRA, Carissan Y, Cooper DL, Cossi M, Fleig T, Fu¨lscher MP, Gagliardi L, de Graaf C, Hess BA, Karlström G, Lindh R, Malmqvist P-Å, Neogrády P, Olsen J, Roos BO, Schimmelpfennig B, Schütz M, Seijo L, Serrano-Andrés L, Siegbahn PEM, Stalring J, Thorsteinsson T, Veryazov V, Wierzbowska M, Widmark P-O (2003) MOLCAS Version 5.2, University of Lund, Lund, Sweden
52. Refson K (2000) Comput Phys Commun 126:310
53. Berendsen HJC, van der Spoel D, van Drunen R (1995) Comp Phys Comm 91:43–56
54. Jorgensen W, Maxwell DS, Tirado-Rives J (1996) J Am Chem Soc 118:11225
55. Jorgensen WL, Chandrasekhar J, Madura JD, Impey RW, Klein ML (1983) J Chem Phys 79:926
56. Chirlian LE, Francl MM (1987) J Comput Chem 8:894
57. Breneman M, Wiberg KB (1990) J Comput Chem 11:316
58. Zuev D, Bravaya KB, Crawford TD, Lindh R, Krilov AI (2011) J Chem Phys 134:034310
59. Gromov E, Burghardt I, Hynes I, Köppel H, Cederbaum LS (2007) J Photochem Photobiol A 190:241
60. Gromov E, Burghardt I, Köppel H, Cederbaum LS (2007) J Am Chem Soc 129:6798
61. Boggio-Pasqua M, Groenhof G (2012) J Phys Chem B 115:7021
62. Putschögl M, Zirak P, Penzkofer A (2008) Chem Phys 343:107
63. Rocha-Rinza T, Christiansenm O, Rajput H, Gopalan A, Rahbek DB, Andersen LH, Bochenkova AV, Granovsky AA, Bravaya KB, Nemukhin AV, Christiansen KL, Nielsen MB (2009) J Phys Chem A 113:9442
64. Nielsen IB, Boye-Peronne S, El Ghazaly MOA, Kristensen MB, Nielsen SB (2005) Anderson LH. Biophys J 89:2597
65. Zuev D, Bravaya KB, Crawford TD, Lindh R, Krylov AI (2011) J Chem Phys 134:034310
66. Gromov EV, Burghardt I, Hynes JT, Köppel H, Cederbaum LS (2007) J Photochem Photobiol A Chem 190:241
67. Muguruza González E, Guidoni L, Molteni C (2009) Phys Chem Chem Phys 11:4556
68. Sergi A, Crüting M, Ferrario M (2001) F Buda J Phys Chem B 105:4386
69. Naseem S, Laurent AD, Carroll EC, Vengris M, Kumauchi, Hoff MWD, Krylov AI, Larsen DS (2013) J Photochem Photobiol A Chem 270:43
70. Wang Y, Li H (2010) J Chem Phys 133:034108